

Residual bond behavior of high strength concrete-filled square steel tube after elevated temperatures

Zongping Chen ^{*1,2}, Xiang Liu ^{1b} and Wenxiang Zhou ^{1c}

¹ College of Civil Engineering and Architecture, Guangxi University, 100# east daxue road, Nanning, 530004, China

² Key Laboratory of Disaster Prevention and Structure Safety of Chinese Ministry of Education, Guangxi University, 100# east daxue road, Nanning, 530004, China

(Received January 16, 2017, Revised March 22, 2018, Accepted March 24, 2018)

Abstract. This paper presents experimental results on the residual bond-slip behavior of high strength concrete-filled square steel tube (HSCFST) after elevated temperatures. Three parameters were considered in this test: (a) temperature (i.e., 20°C, 200°C, 400°C, 600°C, 800°C); (b) concrete strength (i.e., C60, C70, C80); (c) anchorage length (i.e., 250 mm, 400 mm). A total of 17 HSCFST specimens were designed for push-out test after elevated temperatures. The load-slip curves at the loading end and free end were obtained, in addition, the distribution of steel tube strain and the bond stress along the anchorage length were analyzed. Test results show that the shape of load-slip curves at loading ends and free ends are similar. With the temperature constantly increasing, the bond strength of HSCFST increases first and then decreases; furthermore, the bond strength of HSCFST proportionally increases with the anchoring length growing. Additionally, the higher the temperature is, the smaller and lower the bond damage develops. The energy dissipation capacity enhances with the concrete strength raising, while, decreases with the temperature growing. What is more, the strain and stress of steel tubes are exponentially distributed, and decrease from the free end to loading end. According to experimental findings, constitutive formula of the bond slip of HSCFST experienced elevated temperatures is proposed, which fills well with test data.

Keywords: square steel tube; high strength concrete; elevated temperatures test; static test; residual bond strength

1. Introduction

High strength concrete-filled square steel tube (HSCFST) is a composite member that is made of steel tube filled with high strength concrete. The reinforcement theory of HSCFST lies in the confinement effect that steel tube has on core concrete when in axial compression. Meanwhile, due to the inner concrete, the steel tube is able to avoid or postpone local buckling. For high strength concrete, HSCFST has its advantages of high strength and long durability, and avoids its disadvantages of low ductility and poor energy dissipation. HSCFST possesses the merits of high bearing capacity, excellent plasticity and ductility, outstanding anti-seismic property, which could be used in engineering widely (Su *et al.* 2014, Patel *et al.* 2014, Aslani *et al.* 2015).

In the mechanical properties of HSCFST, a creep model, considering the state of triaxial stress and autogenous shrinkage of high strength concrete core, has been proposed by Ma and Wang (2012), which demonstrated that there exists an obvious difference in the creep between HSCFST columns and normal strength concrete filled steel tube

columns. In addition, Lai and Ho (2014) investigated 29 HSCFST columns with different strength concrete and installed with external steel rings subjected to uni-axial compression. They found that the proposed ring installation can further improve both strength and ductility of HSCFST columns by restricting the column dilation. What is more, Guler *et al.* (2014) studied the effect of section shape on the bond behavior under axial load capacity, results showed the circular HSCFST columns have higher bond stress capacity than the square ones. The splitting crack is an important factor affecting the confined concrete. Based on confined specimens with test results published in the literature, Kwan *et al.* (2015) proposed a theoretical model for evaluating the lateral strain, confining stress and axial stress in FRP confined concrete is developed. The same as it, Dong *et al.* (2015) put forward a criterion for formation of splitting cracks has been established and a constitutive model for predicting the lateral strain of confined concrete has been developed. They point out that the lateral strain is dependent only on the axial strain, confining stress and concrete strength. By a new constitutive model for confined ultra-high strength concrete, Wang and Liew (2016) used ABAQUS do the research of compression load versus axial strain and lateral strain curves. Results show that the proposed model can predict accurately the maximum resistance of the stub CFST columns. At last, Yang *et al.* (2017) researched the flexural behavior of HSCFST with inner CFRP (carbon fiber reinforced polymer) circular tube by the ABAQUS/Standard solver, at the same time, eight

*Corresponding author, Ph.D., Professor,
E-mail: zpchen@gxu.edu.cn

^a Ph.D.

^b Ph.D. Student

^c Master

specimens were fabricated and tested to investigate the pure flexural behavior.

Bond behavior is of fundamental importance for the monolithic action in bonded concrete and steel tube, which has great influence on the behavior of HSCFST members. In studying bond strength, push-out tests are applied and average loads are used to calculate average bond strength (El-Hawary and Hamoush 1996). For instance, Xu *et al.* (2009) pointed out that the interfacial bond strength of concrete-filled steel tube (CFST) decreases with the increase of diameter thickness ratio. Shakir-Khalil (1993) studied the influence of roughness of steel tube inner wall on the bond strength. They concluded that with the rougher of the steel tube inner wall, the mechanical joint force and frictional force between the concrete and the steel tube will be greater, and the bond strength will improve. Tao *et al.* (2016) investigated the influence of concrete age, and found that the longer the concrete age, the lower the bond strength. Qu *et al.* (2014) conducted push-out tests and approved that lubricating the steel-concrete interface always had a significant adverse effect on the interface bond strength.

Fire disaster can seriously damage building structure and even lead to its collapse, posing a big threat to the life safety of victims and firemen. Numerous fire resistance study and engineering practice home and abroad show that HSCFST structure possesses pretty good fire resistance (Moliner *et al.* 2013, Xiong and Liew 2016, Schaumann *et al.* 2009, Romero *et al.* 2015). The reasons of good fire resistance may be explained by the interaction between the concrete and steel tube. Tao *et al.* (2011) investigated post-fire bond in concrete filled steel tubular columns with normal concrete and self-consolidating concrete. Song *et al.* (2017) researched bond behavior of normal and expansive

concrete filled steel tubes at elevated temperatures. In these studies, fire exposure time, temperature level, hold time period of heating and loading condition during heating were especially considered as variables compared with related researches without temperature exposure, on the basis, the mutual effect of other factors on post-fire bond behaviors of concrete-filled steel tubes were investigated. However, there is little report on the study of bond behavior of HSCFST after elevated temperature.

Studying the damage mechanism of interface bond behavior of HSCFST and establishing corresponding constitutive equation of bond slip can lay a foundation for the establishment of security evaluation theory of HSCFST and for the development of finite element numerical simulation technology. Therefore, in this paper, the author has designed 17 HSCFST specimens and carries out static push-out experiments after elevated temperatures to analyze failure mechanism and slip characteristics of interface bond.

2. Experimental program

2.1 Specimen detail

As shown in Table 1, four groups of test (17 specimens in all) were designed and conducted. Specimens of group one to three were designed to consider the parameters of concrete strength and elevated temperatures, group four mainly took anchorage length as an effect factor, moreover, there was also a unheated specimen left in room temperature in each group as a contrast. All of the square steel tubes were fabricated from grade Q345 steel, the cross section length (B) of square steel tube was 150 mm, the wall

Table 1 Characteristics of specimens

Group	Specimen No.	Concrete grade	T/°C	t/min	H/mm	l_a /mm	l_a/B
1	HSCFST-01	C60	20	—	450	400	2.667
	HSCFST-02	C60	200	60	450	400	2.667
	HSCFST-03	C60	400	60	450	400	2.667
	HSCFST-04	C60	600	60	450	400	2.667
	HSCFST-05	C60	800	60	450	400	2.667
2	HSCFST-06	C70	20	—	450	400	2.667
	HSCFST-07	C70	200	60	450	400	2.667
	HSCFST-08	C70	400	60	450	400	2.667
	HSCFST-09	C70	600	60	450	400	2.667
	HSCFST-10	C70	800	60	450	400	2.667
3	HSCFST-11	C80	20	—	450	400	2.667
	HSCFST-12	C80	200	60	450	400	2.667
	HSCFST-13	C80	400	60	450	400	2.667
	HSCFST-14	C80	600	60	450	400	2.667
	HSCFST-15	C80	800	60	450	400	2.667
4	HSCFST-16	C80	20	—	300	250	1.667
	HSCFST-17	C80	400	60	300	250	1.667

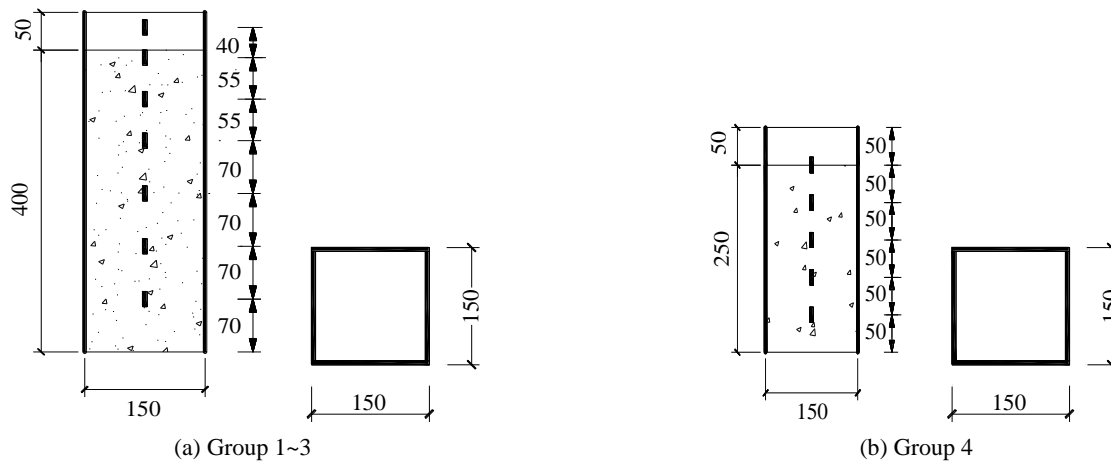


Fig. 1 Dimensions of specimens

Table 2 Concrete mix proportions

Concrete grade	Material content /(kg/m ³)							Collapsibility
	Cement	Sand	Gravel	Water	Fly ash	Silica fume	Water reducer	
C60	400	600	1280	165	60	4.0	5	7.5
C70	450	680	1128	160	70	5.0	7	6.0
C80	520	628	1117	155	80	5.5	9	6.0

Table 3 physical properties of gravel and sand

Aggregate	Crushing index (%)	Fineness modulus	Apparent density (kg/m ³)	Bulk density (kg/m ³)	Voidage (%)	Mud content (%)	Drinking rate (%)	Moisture content (%)
Gravel	12.5	—	2702	1520	43.74	1.08	0.373	0.013
Sand	—	3.02	2637	1579.2	40.11	0.94	0.654	0.285

thickness was 5 mm. According to the length of the steel-concrete interface l_a and the air gap at the top end of specimens prepared for the measurement of slip, as presented in Fig. 1, the tubes were cut smoothly in workshop, prior to concrete casting. No fire prevention and de-rusting treatment were taken to the outside and inner surfaces of the tubes, respectively.

2.2 Material properties

P.O 42.5 ordinary portland cement, well-graded small and medium-size river sand and gravel of 5~25 mm diameter were used in the test. Naphthalene-based water reducer, first-grade fly ash as well as silica fume were used as admixture; urban tap water was used in this test. The concrete mix proportion and physical property of aggregates is shown in Tables 2 and 3, respectively. Standard cubes (150 mm × 150 mm × 150 mm) were cast, cured, and heat treated under similar conditions, then tested to evaluate compressive strength. The cube compression strength of C60, C70 and C80 concrete unheated was 61.8, 70.2 and 81.9 MPa respectively. The yield strength of steel cube was 366.8 MPa and its ultimate tensile strength was 467.5 MPa.

2.2 Material properties

P.O 42.5 ordinary portland cement, well-graded small and medium-size river sand and gravel of 5~25 mm diameter were used in the test. Naphthalene-based water reducer, first-grade fly ash as well as silica fume were used as admixture; urban tap water was used in this test. The concrete mix proportion and physical property of aggregates is shown in Tables 2 and 3, respectively. Standard cubes (150 mm × 150 mm × 150 mm) were cast, cured, and heat treated under similar conditions, then tested to evaluate compressive strength. The cube compression strength of C60, C70 and C80 concrete unheated was 61.8, 70.2 and 81.9 MPa respectively. The yield strength of steel cube was 366.8 MPa and its ultimate tensile strength was 467.5 MPa.

2.3 Test setup and loading process

As provided in Fig. 2, temperature exposure treatment of specimens was carried out in a RX3-45-9 electric oven, which had an automated device to control temperature rise rate, and all the specimens was exposed to fire on its four surfaces (upright placing) in the furnace. According to the



Fig. 2 Heated equipment

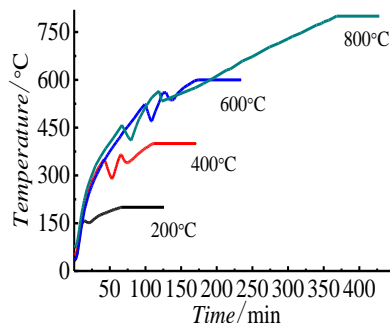


Fig. 3 Heating curves

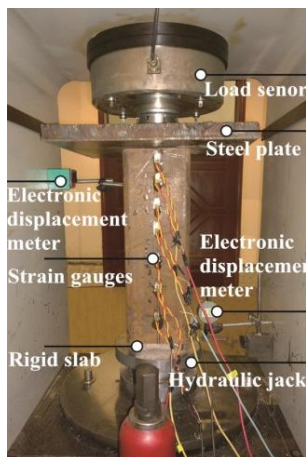


Fig. 4 Test setup

equipment's performance parameter, the heating rate was set to about $10^{\circ}\text{C}/\text{min}$, when it reached the target temperature for each group specimen, the temperature would be automatically constant. The heating curves were measured as given in Fig. 3. On the basis of the *Fire Resistance Rating in Code for Fire Protection Design of Building*, the constant temperature time (t) was set to be 60 minutes for all specimens heated. After elevated temperature, the specimen is shelved for a week till the test when the specimen reaches the room temperature in the opened furnace.

As shown in Fig. 4, RMT-201 rock and concrete mechanics test system was used to do the push-out test on specimen after elevated temperatures. The specimens were set up in the testing machine with the air gap at the top. To allow the concrete core to be pushed up through the tube

when testing, two steel blocks were used. At the bottom loading end, one steel block, which had a cross-section slightly smaller than the inner diameter of square steel tube, was adopted to make sure the load to be applied only on the core concrete, meanwhile, another steel block were used to resist the steel tube with the air gap at the top free end, which assure the load were transferred only by steel tube. The relative slip between the core concrete and square steel tube was both measured by electronic displacement meter. In order to measure the slip of the free end at the top, prior to concrete casting, a 10 mm wide perpendicular was cut on the 50 mm reserved hollow steel tubes at the top end of specimen, and then a thin steel bar with high stiffness was embedded in the steel tube with concrete through the perpendicular, which were used to place the electronic displacement meter. And the slip of the loading end at the bottom were measured by the electronic displacement meter located at the bottom steel block. Axial strain in the steel tube were measured using strain gauges installed along the length of the steel tube, and the strain gauges were spaced at a range of 40-70 mm intervals as shown in Fig. 1.

In order to eliminate instruments' touch errors, every time prior to the bonding test, pre-loading, which was 10% of the estimated value of ultimate load, would be done three times. This can ensure that equipment and instruments function properly. All specimens were tested under monotonic load with the loading rate of 0.002 mm/s . The push-out load (P) and slips (S) at both the loading end and free end of testing specimens were measured in order to determine a load-slip relationship. When the slip at the free end of the specimen was quite large and the corresponding load did not have obvious change any more, the test was ended.

3. Experiment results and analysis

3.1 Phenomenon after elevated temperatures

Compared with specimens unheated, the surface color of specimens after elevated temperatures changed, accompanying with cracks on both open ends of specimens. Take specimens of C80 concrete for example. Unheated specimen HSCFST-11 ($T = 20^{\circ}\text{C}$) was sandy beige with no crack at all on the surface; while exposed temperatures elevated, like $T = 200^{\circ}\text{C}$, specimen HSCFST-12 turned yellow with no crack on the surface of the concrete; when $T = 400^{\circ}\text{C}$, specimen HSCFST-13 became sorrel and obvious crack appeared at the end of the concrete. As the temperature rose, the color of concrete gradually turned dark and the width and depth of the crack developed wider. When $T = 600^{\circ}\text{C}$, specimen HSCFST-14 turned rufous and crack became wider; when $T = 800^{\circ}\text{C}$, specimen HSCFST-15 turned bronzing which was the darkest and concrete peeling appeared on the surface. The cracks at the end of the concrete and the exterior color of specimens after elevated temperatures are illustrated in Figs. 5 and 6.

3.2 Mass loss rate

The calcium silicate hydrate gel in HSC dehydrates an

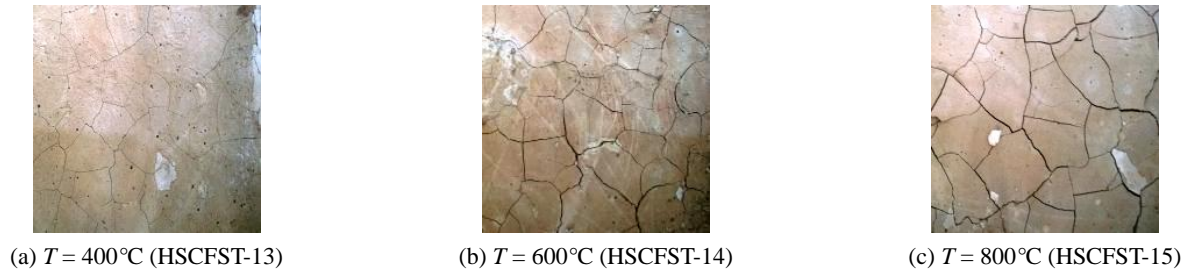


Fig. 5 Concrete cracks after elevated temperatures

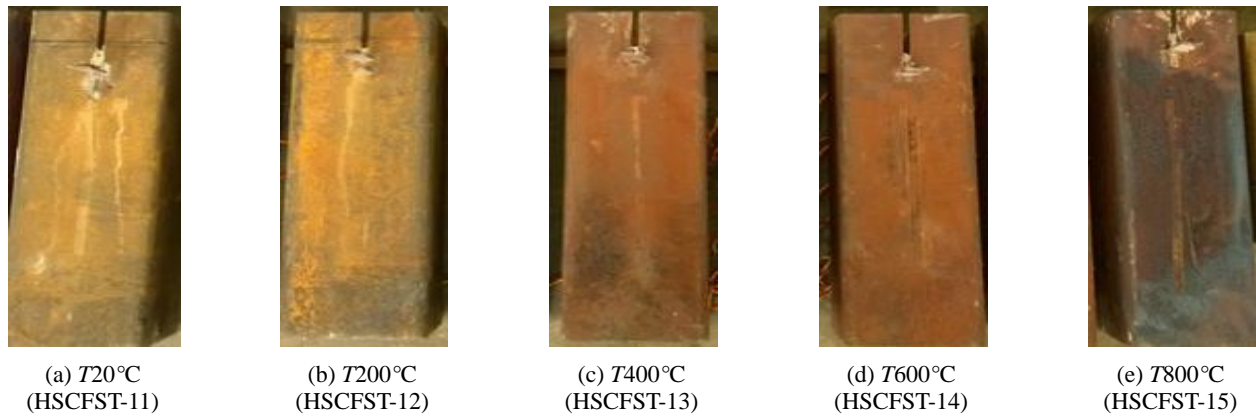


Fig. 6 Surfacecolor of specimens after elevated temperatures

decomposes and some combustible components burn after elevated temperatures, which leads to the deterioration of mechanical property of concrete. By measuring the weight of specimens before and after elevated temperatures, mass loss rate (I) is acquired. The calculating formulas is

$$I = \frac{M - M_f}{M} \times 100\% \quad (1)$$

where I is mass loss rate, M is the weight of specimens before temperature exposures and M_f is the weight after temperature exposures.

The changing graph of mass loss rate is shown in Fig. 7. It can be seen from Fig. 7, mass loss rate increases with the rise of temperature. When $T = 200^\circ\text{C}$, mass loss rate is between 0.5%~0.9%; when $T = 400^\circ\text{C}$, the figure is about 3.5%; when $T = 800^\circ\text{C}$, it reaches 4.5%~6%. When temperature rises from 200°C to 400°C , mass loss rate changes dramatically, as once $T > 200^\circ\text{C}$, the remaining

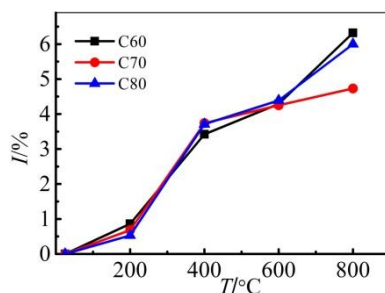


Fig. 7 Mass loss rate varies with the constant temperatures

water in concrete evaporated greatly and a large amount of calcium silicate hydrate gel dehydrated and decomposed. This was in line with the experimental phenomenon. That is, when $T = 400^\circ\text{C}$, a large amount of fog emitted from the gap in resistance furnace.

3.3 Push-out experiment phenomenon

For all specimens, the slip started from the load end. Along with the increase of push-out load, the slip expanded gradually to the free end. In terms of specimens unheated, when the load reached around $80\%P_u$ (P_u is the ultimate load), the specimens gave out the sound of rub-a-dub, after that, the load surged and reached the ultimate load, then the load declined considerably and finally remained constant. At the end of push-out test, there was no obvious difference of P - S curves between loading and free ends. The specimens after elevated temperatures didn't make any noise during the loading process. For specimens after elevated temperatures of 600°C and 800°C , when they were loaded to $60\% \sim 80\% P_u$, peeling appeared on the outer surface of the square tubes at the free end and then obvious slip line developed as well. The slip line formed an angle of approximately 45° with the perpendicular line of square tubes (positive and negative intersection). For specimens after elevated temperatures of less than 600°C , no slip line appeared. With the loading increased, the slip line gradually expanded from the free end to load end. After loading, specimens were observed. It was found that the concrete at the load end of specimens under different temperature slipped $5 \sim 10$ mm and the wall of tubes bent outward and even out of shape. The slip line and failure mode at the load end are illustrated in Fig. 8.



(a) Slip line



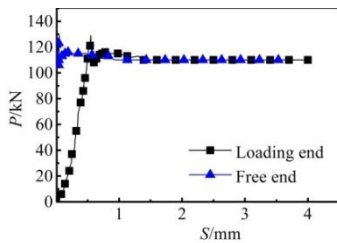
(b) Failure model of loading end

Fig. 8 Phenomenon of slip line and loading end

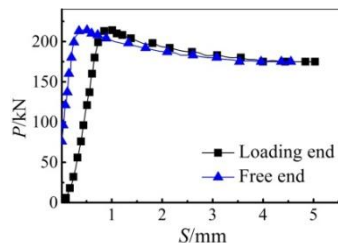
3.4 Load-Slip (P - S) curves

Fig. 9 shows the typical curves of push-out load versus slip at both the loading and free end for HSCFST specimens. Apparently, it can be found that there were some

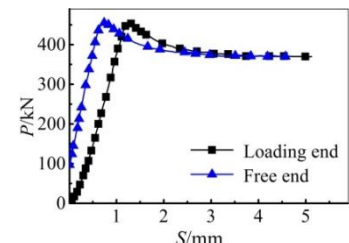
noticeable features for load-slip curves at both ends, especially in the stage before attaining the ultimate bond strength. P - S curves of load end can be divided into three sections: upward section, downward section and horizontal plateau. P - S curves of free end can be divided into four



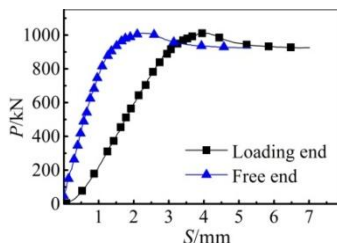
(a) HSCFST-1



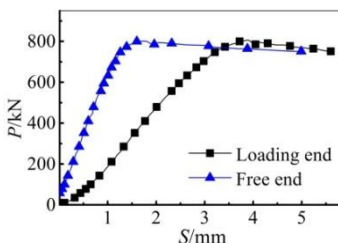
(b) HSCFST-2



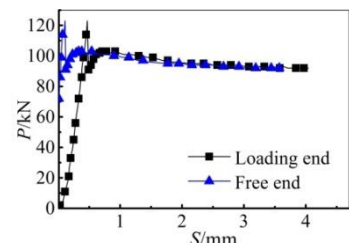
(c) HSCFST-3



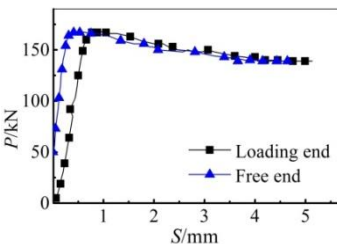
(d) HSCFST-4



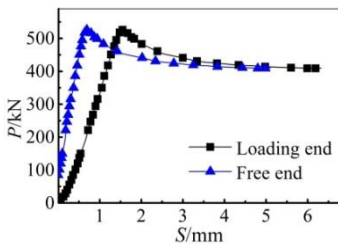
(e) HSCFST-5



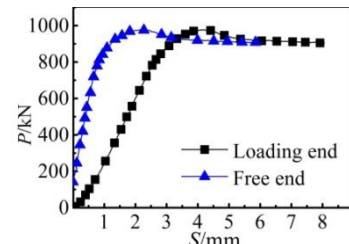
(f) HSCFST-6



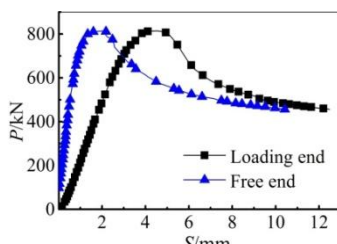
(g) HSCFST-7



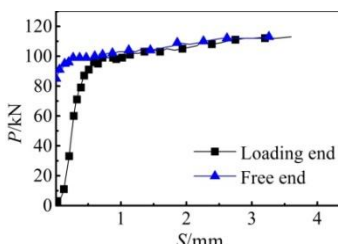
(h) HSCFST-8



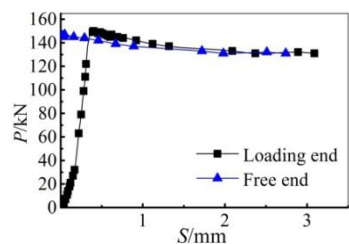
(i) HSCFST-9



(j) HSCFST-10



(k) HSCFST-11



(l) HSCFST-12

Fig. 9 Load-slip curves of specimens

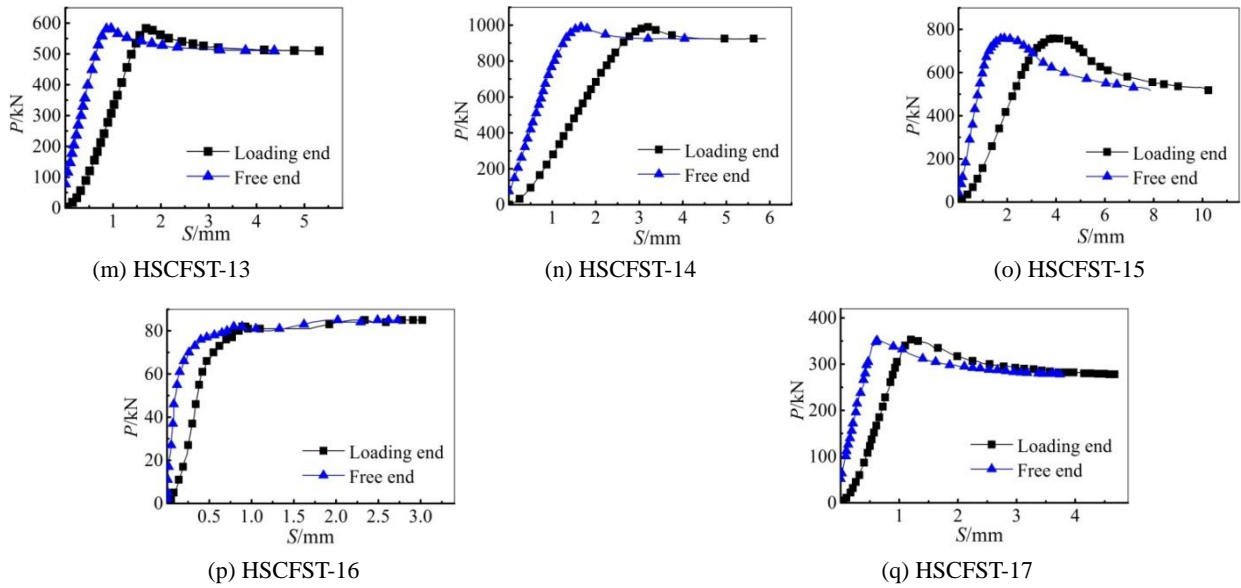


Fig. 9 Continued

sections: no slip section, upward section, downward section and horizontal plateau.

- (1) Upward section: at the beginning of loading, the bond force of specimens is mainly provided by chemical adhesion force. The relative slip between HSC and square steel tube is caused by the shear deformation of interface layer. The bond stress increases linearly with the shear deformation of interface layer become larger. In the experiment, the curves' slope of some exceptional specimens reduces gradually in the upward section, showing a rising curve. This is because when bond stress increases to a specific point, micro cracks emerge on the interface layer which becomes wider with the increase of load, contributing to the stiffness deterioration of interface bond slip.
- (2) Downward section: when loaded to the peak load, shear failure on the contact interface between HSC and square steel tube appear and chemical adhesion force lost. By this time, the function of mechanical interlocking and friction enhances to replace the lost chemical adhesion force. Fretting wear behavior emerges on the interface of square steel tube and HSC. Tube and the tiny embossments on the surface of concrete occlude each

each other, which bring about mechanical interlocking. In the occlusion, the concrete embossments with less strength firstly fail in shear and then fractures, leaving concrete debris on the contact interface. Concrete debris deposit on the surface and friction coefficient declines. As the further increase of load, concrete embossments fracture one after another, leaving more and more debris. This gradually contributes to the loss of mechanical interlocking. Finally, the steel surface is filled and leveled up by debris and then friction coefficient becomes constant. In the later period of downward section, bond force is only provided by interface friction.

- (3) Horizontal plateau: in this period, the frictional wear on the interface between HSC and square tubes is basically constant. Normal stress on the surface and friction resistance caused by normal stress is close to constant value. Bond stress tends to be constant but slippage continues to increase. P - S curve is close to a horizontal line.

All the curves of load ends are divided into three categories shown in Fig. 10. All the three types consist of three periods - OA , AB and BC , among which OA is upward section and BC is slow downward section. In terms of AB ,

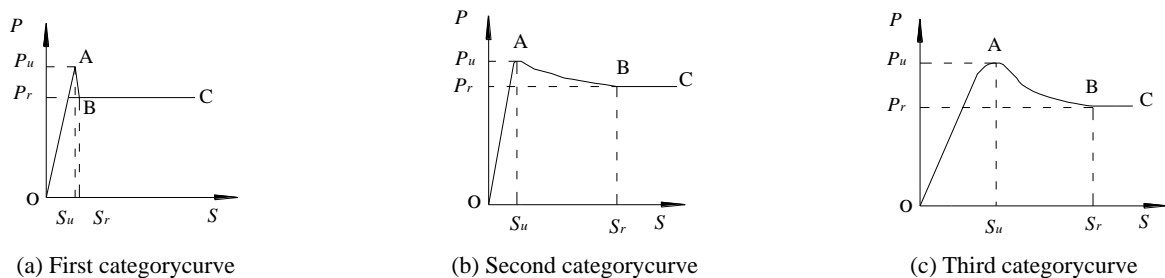


Fig. 10 Typical classification of load-slip curves

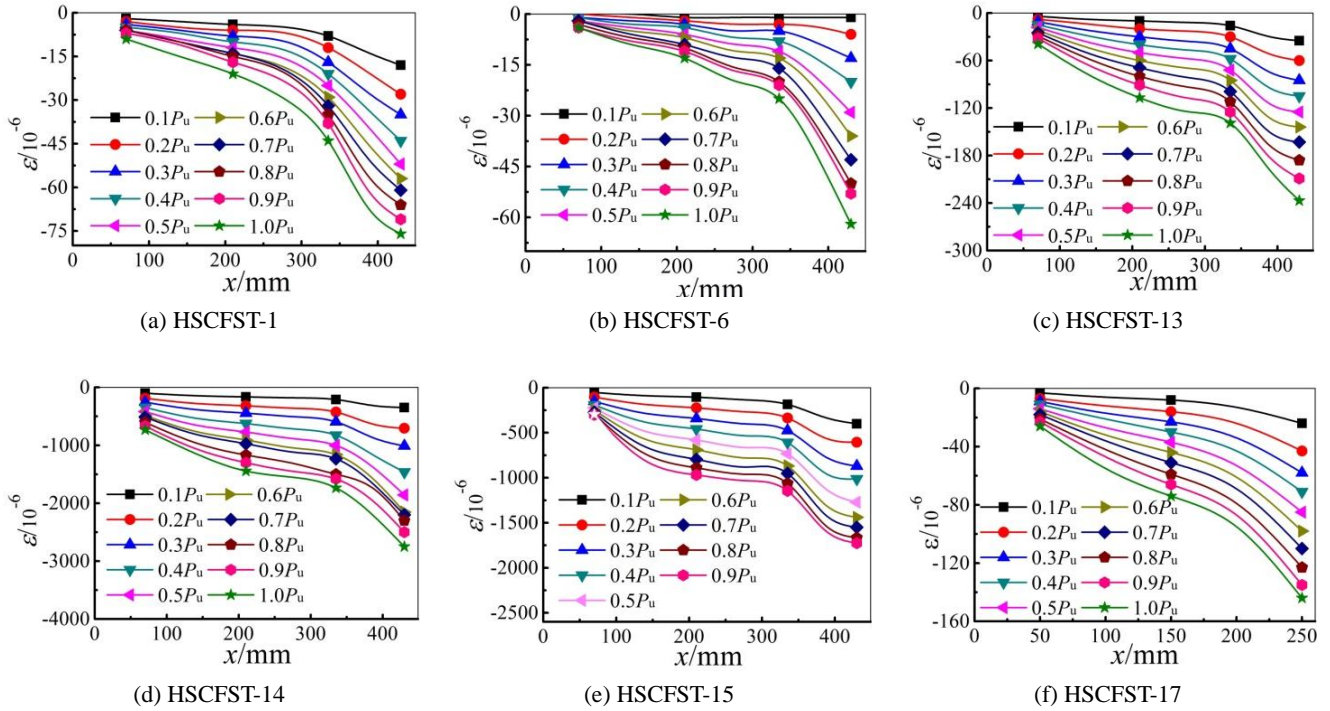


Fig. 11 Longitudinal strain distribution along steel tube curves

the curve of the first category drops sharply. To be more specific, it falls suddenly when reaches the ultimate load. The slippage S_u corresponding to the ultimate load P_u and the slippage S_r corresponding to the residual load P_r are quite small. Unheated specimens HSCFST-1 and HSCFST-6 are likely to form this curve. In the curve of second type, AB declines gradually. Specifically, the curve drops slowly when it reaches the ultimate load with fairly small S_u but quite big S_r . Specimens under $T = 200^\circ\text{C}$ and 400°C are prone to form this curve. In terms of the curve of third category, AB also declines gradually. In detail, the curve drops slowly when it reaches the ultimate load with both fairly big value of S_u and S_r . Specimens under $T = 600^\circ\text{C}$ and 800°C are likely to form this curve. Thus it can be seen, as temperature rises, the curve transforms from the first category to the third one, brittleness becoming weakened while ductility becoming strengthened.

3.5 Longitudinal strain distribution along steel tube

Fig. 11 illustrates the longitudinal strain distribution along steel tube in the upward section of specimens HSCFST-1, HSCFST-6, HSCFST-13, HSCFST-14, HSCFST-15 (the value at $1.0P_u$ was missed) and HSCFST-17, x is the distance between measure point and load end.

It can be seen from Fig. 11, at the beginning of loading, strain presents roughly exponential distribution along the cube. According to the conversion relations between stress and strain at the elastic stage of steel, the bond stress between square steel tube and HSC can be drawn as the Eq. (2)

$$\tau(x) = \frac{E_s A_s}{L} \frac{d\varepsilon_x}{dx} \quad (2)$$

where $\tau(x)$ is the bond stress at x ; E_s is the steel elastic

Table 4 Characteristic values of specimens

Specimen No	P_u/kN	P_r/kN	τ_u/MPa	τ_r/MPa	Specimen No	P_u/kN	P_r/kN	τ_u/MPa	τ_r/MPa
HSCFST-1	132	110	0.59	0.49	HSCFST-10	816	456	3.64	2.04
HSCFST-2	217	175	0.97	0.78	HSCFST-11	115	113	0.51	0.51
HSCFST-3	456	370	2.04	1.65	HSCFST-12	151	131	0.67	0.59
HSCFST-4	1013	926	4.52	4.13	HSCFST-13	583	510	2.60	2.28
HSCFST-5	812	751	3.63	3.35	HSCFST-14	991	925	4.42	4.13
HSCFST-6	124	92	0.55	0.41	HSCFST-15	747	494	3.33	2.21
HSCFST-7	170	139	0.76	0.62	HSCFST-16	87	85	0.62	0.61
HSCFST-8	530	410	2.37	1.83	HSCFST-17	355	278	2.53	1.98
HSCFST-9	979	905	4.37	4.04					

modulus; A_s is the sectional area of steel tube; L is the sectional perimeter of steel tube.

3.6 Characteristic parameter of load-slip curve

Table 4 illustrates all specimens' characteristic values. The paper defines the load at the peak point in the load-slip curve as the ultimate load (P_u), and the load at the horizontal plateau is called residual load (P_r). At present, in the researches home and abroad about steel and concrete bond behavior, there have not been any uniform standards for the definition of bond strength. In the paper, the interfacial shear stress related with P_u is defined as bond strength τ_u , while the interfacial shear stress matched with P_r is called residual bond strength τ_r . The formulas are

$$\tau_u = \frac{P_u}{sl_a} \quad (3)$$

$$\tau_r = \frac{P_r}{sl_a} \quad (4)$$

where τ is the bond strength, MPa; P is the value of load, kN; s is the perimeter of contact interface, mm; l_a is the anchorage length, mm.

The design and criteria for interface bond strength of concrete-filled square steel tube vary in different countries. AIJ (1997) in Japan defines the design value of bond strength as 0.15 MPa; while both BS 540025 (2005) in Britain and BS EN 1994-1-1 (2004) in Europe define it as 0.4 MPa. It can be seen from Table 3, after elevated temperatures, τ_u (0.51~4.52 MPa) and τ_r (0.41~4.13 MPa) of HSCFST can meet the corresponding requirements.

4. Factors influence on bond strength

4.1 The exposure temperature

The bond strength curves of HSCFST after elevated temperatures changing along with temperature T are shown in Fig. 12. It can be seen from Fig. 12, as the increase of T , all the specimens' bond strength $\bar{\tau}_u$ and residual bond strength $\bar{\tau}_r$ increase first and then drop. (Average values are extracted from specimens at the same T regardless of their concrete strength grades.) The bond strength and residual bond strength of specimens after 600°C are the

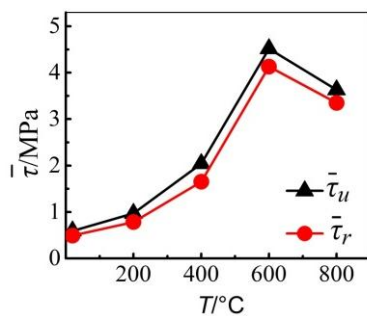


Fig. 12 Effect of constant temperature on bond strength

highest among all the groups. Their values of $\bar{\tau}_u$ and $\bar{\tau}_r$ are 8.4 times as much as those unheated. The bond strength of specimens at $T = 800^\circ\text{C}$ is less than that at $T = 600^\circ\text{C}$, whose value of $\bar{\tau}_u$ and $\bar{\tau}_r$ are 6.4 times and 5.4 times as much as those unheated, respectively.

The bond strength increases first and then decreases along with temperature, which is higher than that in normal temperature. Yet in the Paper Chiang and Tsai (2003) and Haddad and Shannis (2004), according to steel bar pull-out test and structural steel push-out test after high temperature, bond strength between steel bar as well as structural steel and concrete decreases, decrease rate becoming larger as temperature increases, which is very different from the experimental results in the paper.

There are some reasons for the differences. (1) After elevated temperatures, a range of physiochemical process emerges in the concrete, leading to its functional deterioration which gives rise to the reduction of chemical adhesion force between concrete interface and steel tube. (2) Following the principle of heat-expansion and cold-contraction, the volume of concrete and tube expands during heating process while it contracts when the specimens cooling down. The expansion of concrete brings about many cracks in it. The irreversibility of cracks results in concrete's shrinkage less than tube's shrinkage. Therefore, the concrete hinders the contraction of the tube, thus extrusion pressure happens between the tube and concrete. (3) The higher the temperature is, the more extrusion pressure is after cooling. Therefore, mechanical interlocking and friction are bigger consequently.

The result was also contrary to the research of Schaumann and Kleiboemer (2017). According to their paper, the bond strength of CFTES at room-temperature is greater than that of CFTES which is heated. This is because the push-out test is carried out at high temperature, when both steel core and concrete cover are thermal expansion. However, the test of HSCFST is conducted after elevated temperature, in which both steel tube and high strength concrete experienced thermal expansion and shrinkage, then, the difference between the volume shrinkage leads to the emergence of extrusion pressure, therefore, the bond strength increases.

When $T \leq 600^\circ\text{C}$, due to the contraction difference of tube and concrete, the higher the temperature is, the higher the interface bond strength and residual bond strength are.

When $T = 800^\circ\text{C}$, as too high temperature results in strength loss of concrete and brittle augment, the concrete within certain thickness range on the interface is easily to

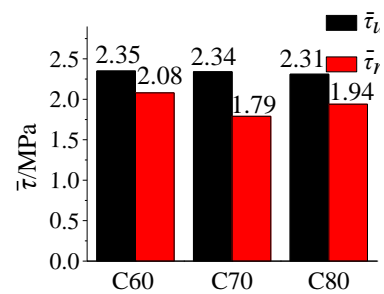


Fig. 13 Effect of concrete strength on average bond strength



Fig. 14 Effect of anchorage length on bond strength

crush. When small slip emerges between concrete and tube, the concrete crush within certain thickness range is ground into tiny particles, forming a rolling friction layer. That's why bond strength and residual bond strength go down at the same time.

4.2 Concrete strength

Fig. 13 is the bar graph on bond strength and residual bond strength of specimens with different strengths after high temperature. (In the analysis average values are extracted from specimens at the same strength grade regardless of exposure temperatures.) It can be seen from Fig. 13, as the increase of concrete strength, there is little change in bond strength and residual bond strength.

4.3 Anchorage length

According to Tao *et al.* (2011), for those square specimen with fire exposure time of 90 min and 180 min, the trend is that τ_u increased with increasing l_a/D ratio. As for specimens in this research suffered for 60 min temperature exposure, the influence of anchorage length on bond strength is illustrated in Fig. 14. Under the same concrete strength, bond strength and residual bond strength of HSCFST decrease with the increase of anchorage length. When anchorage length l_a increases from 250 mm to 400 mm, for specimens at $T = 20^\circ\text{C}$, its $\bar{\tau}_u$ decreases by 11.3%, and $\bar{\tau}_r$ declines by 22.9%; for specimens at $T = 400^\circ\text{C}$, its $\bar{\tau}_u$ decreases by 7.5% and $\bar{\tau}_r$ declines by 3.0%. Bond strength of HSCFST decreases with the increase of anchorage length, which is in line with the bond behavior of normal strength concrete-filled steel tubes. Apart from that, the falling range of bond strength in room temperature is larger than that after elevated temperatures. With the increase of temperature, the influence of anchorage length on bond strength tends to be less.

5. Influence of elevated temperature on interface bond failure

5.1 Influence on interface damage

In order to describe quantitatively specimens' damage process and analyze the impact of elevated temperatures on interface bond damage, according to the definition of

damage proposed by Xu *et al.* (2013), a corresponding expression is drawn as

$$D = 1 - \frac{K_t}{K} \quad (5)$$

where K_t is the tangent slope of any point in P - S curve at the load end and K is the bond shear stiffness on the elastic stage.

At the beginning of loading, interface bond is on elastic stage and it can be regarded no bond damage, namely $D = 0$; when it is loaded to elastic-plastic stage, bond damage emerges and the value of D is between 0 to 1; when loaded to peak load, bond shear stiffness becomes negative value, $D = 1$ at this moment. Fig. 15 shows the process that 5 specimens' bond damage D changes along with relative slippage S/l_a . It can be seen from Fig. 15, on the premise that other parameters are the same, the damage of specimens unheated emerges the earliest, while the damage of specimens at 600°C and 800°C emerges the latest. When $T \leq 400^\circ\text{C}$, the damage of specimens develops rapidly, while the damage of specimens at 600°C and 800°C develops slowly. This is the result of residual expansion deformation produced by concrete after cooling and confinement effect caused by the compression that the exterior steel tube produces on inner core concrete. Affected by normal pressure, the development space of defects like crack and gap is compressed, thus the development of defects slows down.

5.2 Influence on interface energy dissipation

The bond failure of HSCFST is accompanied by energy

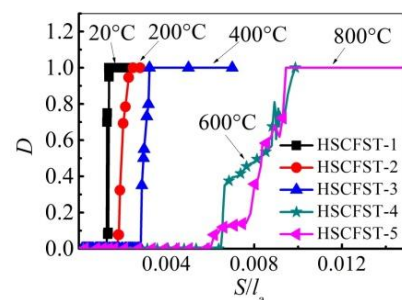


Fig. 15 Bond damage varies with relative slip at loading end

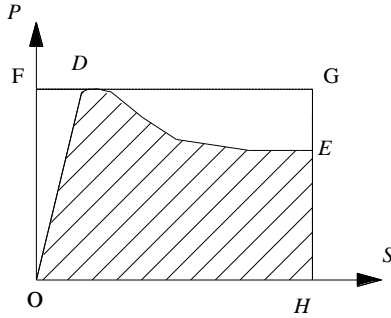


Fig. 16 Energy dissipation area model

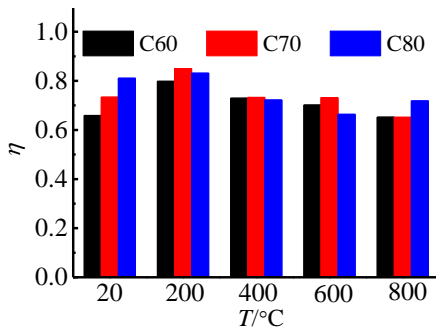


Fig. 17 Energy dissipation factor

absorption and consumption. When HSCFST is loaded and bond slip emerges, the interface will experience the stage of closure of micro cracks, extension of defects and failure. In the process mentioned above, the interface transforms outside mechanical energy to its own performance of elastic-plastic deformation and releases the energy to outside in the form of sound and thermal radiation. In order

to study the energy variation of interface bond behavior of HSCFST after elevated temperatures, energy dissipation factor η is adopted to quantitatively describe energy dissipation capacity. The definition of η is as following

$$\eta = \frac{S_{ODEC}}{S_{OFHG}} \quad (6)$$

where S_{ODEC} is the shaded area in Fig. 16 and S_{OFHG} is the area of rectangle $OFHG$.

Fig. 17 is the bar graph of all specimens' energy dissipation factors. As shown in it, with the increase of temperature, energy dissipation factors firstly increase and then decline. For specimens at $T = 200^\circ\text{C}$, their energy dissipation factors are the biggest, while the energy dissipation factors of specimens at $T = 800^\circ\text{C}$ are the smallest. Except some exceptional specimens, as other parameters are the same, the higher the strength grade of concrete is, the larger the energy dissipation is. Thus it can be seen, in general, the energy dissipation of interface bond increases with the increase of concrete strength and declines with the increase of temperature.

6. Bond stress distribution

By statistical regression of measured strain data and fitting in exponential function, the strain distribution of different load grade along the steel tube length was obtained, which is illustrated in Fig. 18.

It can be seen from Fig. 18, steel tube strain roughly presents exponential distribution along the specimen length. That is to say, ε_x is the exponential function of x

$$\varepsilon_x = ae^{bx} + c \quad (7)$$

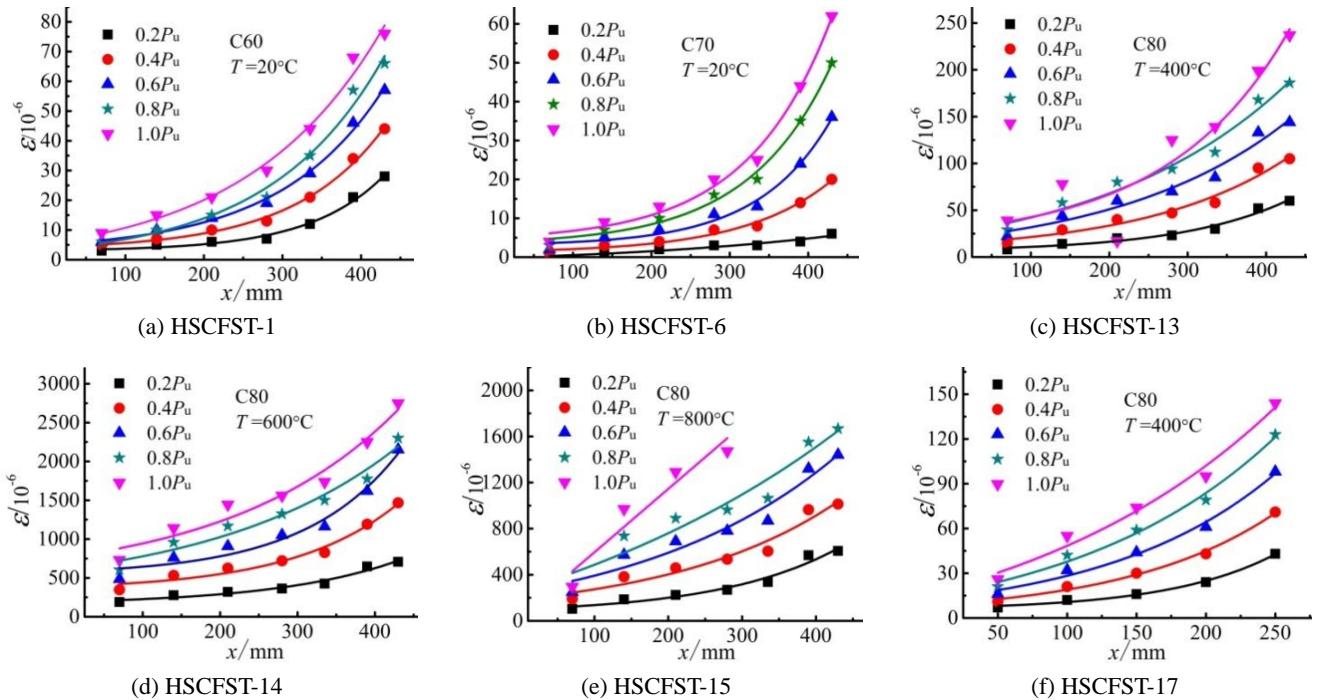


Fig. 18 Strain distribution along steel length direction

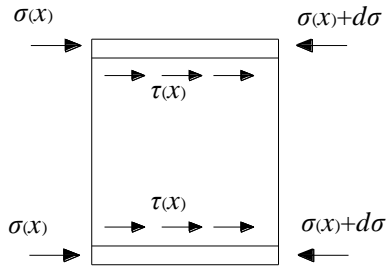


Fig. 19 Stress distribution along the micro steel

where a , b and c are characteristics values of strain distribution of steel tube. The characteristic values of the same specimen with different loads are various. The specific values can be obtained by statistical regression of measured strain distribution. To explain this, according to the force analysis of a certain length of steel tube (Fig. 19), an equilibrium equation is established.

$$\sigma(x) + d\sigma = \tau(x)Ldx + \sigma(x) \quad (8)$$

$$\tau(x) = \frac{d\sigma}{Ldx} \quad (9)$$

$$d\sigma = E_s A_s d\varepsilon_x \quad (10)$$

Eq. (10) is substituted into Eq. (9) and the expression between bond stress and steel tube strain is expressed as the following

$$\tau(x) = \frac{E_s A_s}{L} \frac{d\varepsilon_x}{dx} \quad (11)$$

Eq. (6) is substituted into Eq. (11)

$$\tau(x) = \frac{abE_s A_s}{L} e^{bx} \quad (12)$$

where $\tau(x)$ is the bond stress at x ; E_s is the elastic modulus of steel tube; A_s is the cross-sectional areas of steel tube; L the perimeter of section of steel tube.

It can be found in Eq. (12), bond stress also present exponential distribution along steel tube length.

Fig. 20 illustrates the bond stress distribution of steel tube specimen along steel tube length. It can be seen from Fig. 20, the interface bond stress at the free end of specimen (the direct force end of tube) is the biggest and it declines from the direct force end of tube to that of concrete. The result that bond stress is the biggest at the direct force end of tube is obtained by differential equation. However, according to geometrical condition, there is no interaction force between steel tube and concrete at the free end of the specimen. Specifically, according to boundary condition, bond stress is zero at the direct force end of steel tube, which is in contradiction with the result obtained by differential equation. This is due to a certain degree of random errors existing in the assumption of exponential distribution of the premise strain. It can be seen from Fig. 20, the more the load is, the more the corresponding bond stress is.

7. Constitutive models of bond-slip

The slip value S of the loading end and the specimen's bond stress τ are adopted to establish the constitutive model between bond strength and slippage of HSCFST after elevated temperatures. The P - S curves at the loading end of all specimens are mainly divided into three sections, namely straight rising section, bend descent section and horizontal

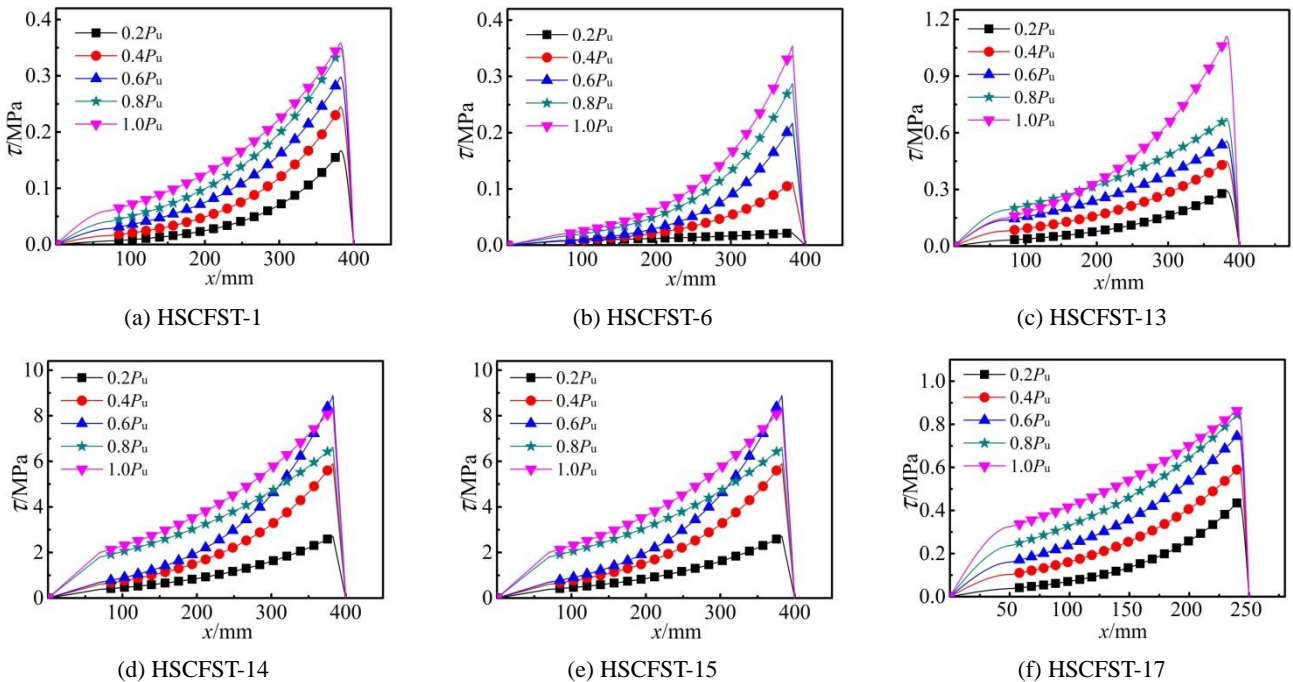


Fig. 20 Bond stress distribution along steel embedment length

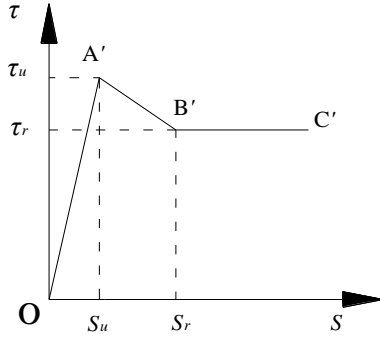


Fig. 21 Three lines model of constitutive relation

section. In order to facilitate the analysis, the constitutive model is simplified to three sections shown in Fig. 21, in which OA' is the straight rising section, $A'B'$ is the descent section and $B'C'$ is the horizontal section. By calculating, the constitutive equations are expressed as the following

$$\tau = \begin{cases} \frac{\tau_u}{S_u} S & (0 \leq S \leq S_u) \\ \frac{\tau_r - \tau_u}{S_r - S_u} S + \frac{\tau_u S_r - \tau_r S_u}{S_r - S_u} & (S_u < S \leq S_r) \\ \tau_r & (S_r > S) \end{cases} \quad (13)$$

where, τ is the bond stress, MPa; S is the slippage at the loading end, mm; τ_u is the bond strength whose value is calculated by Eq. (14), MPa; τ_r is the residual bond strength whose value is calculated by Eq. (15), MPa; S_u is the slippage in accordance with the peak load whose value is calculated by Eq. (16), mm; S_r is the slippage corresponding

to the initial residual load and is calculated by Eq. (17), mm. The parameters τ_u , τ_r , S_u and S_r are based on experimental data and extracted by mathematical fitting as the following

$$\tau_u = -9.92 \times 10^{-3} T + 5.461 \times 10^{-5} T^2 - 4.47 \times 10^{-8} T^3 - 2.18 \times 10^{-3} f_{cu} - 0.08 \frac{B}{l_a} + 0.94 \quad (14)$$

$$\tau_r = -1.26 \times 10^{-2} T + 6.17 \times 10^{-5} T^2 - 5.41 \times 10^{-8} T^3 - 6.88 \times 10^{-3} f_{cu} - 0.267 \frac{B}{l_a} + 1.47 \quad (15)$$

$$S_u = -7.4 \times 10^{-3} T + 3.59 \times 10^{-5} T^2 - 2.67 \times 10^{-8} T^3 - 7.23 \times 10^{-3} f_{cu} + 0.44 \frac{B}{l_a} + 1.16 \quad (16)$$

$$S_r = 1.94 \times 10^{-3} T + 1.82 \times 10^{-5} T^2 - 1.94 \times 10^{-8} T^3 + 3.9 \times 10^{-3} f_{cu} + 0.29 \frac{B}{l_a} + 1.89 \quad (17)$$

Contrastive graphs of calculated data and test data are illustrated in Fig. 22. Concrete strength, temperature and ratio of height to width are taken into account in the constitutive equations in Eq. (13). The characteristic values in constitutive relation graphs are calculated by the formula based on regression fitting of experimental data. Thus, there are differences from the constitutive model which directly adopts experimental data as characteristic points. It can be found in Fig. 22, except some residual bond strength of specimens under high temperature differentiates greatly from test data, the rest specimens fit quite well.

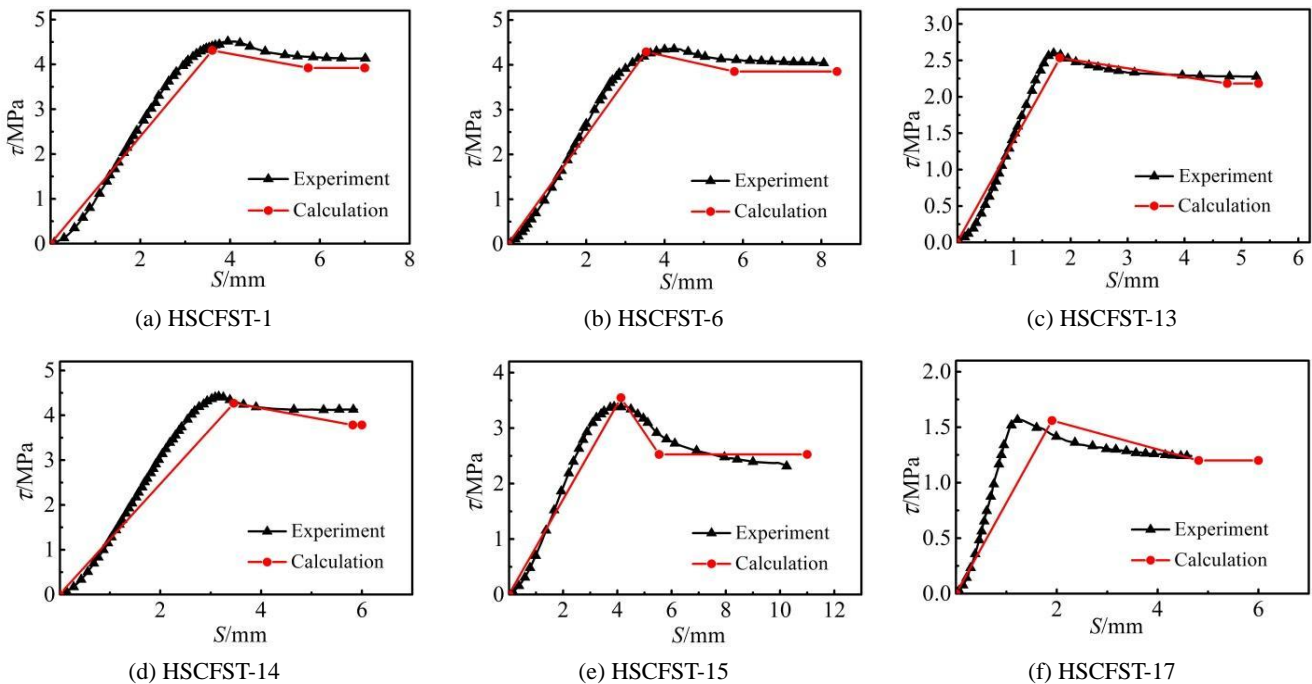


Fig. 20 Bond stress distribution along steel embedment length

8. Conclusions

The effects of concrete strength, temperature and anchorage length on bond strength of high strength concrete-filled square steel tube after elevated temperatures were investigated. The specimens were designed and tested under push-out loading. From the experimental investigated, the following conclusions can be drawn:

- (1) As the increase of temperature, both the slippage in accordance with the peak load and the slippage at the starting point of residual load go up. What is more, the downward section of the Load-Slip curve becomes smooth and slow with weakening brittleness and strengthening ductility.
- (2) For specimens of HSCFST after elevated temperatures, the load-slip curve at the loading end is similar to that at the free end. The emergence of slip at the loading end is earlier than that at the free end.
- (3) Taking 600°C as boundary, when temperature rises from normal to 600°C, bond strength and residual bond strength increase; while they decline when temperature reaches 600~800°C.
- (4) After elevated temperatures, the bond strength of HSCFST is inversely proportional to anchorage length. As exposure temperature goes up, the impact of anchorage length on bond strength gradually reduces. For HSCFST specimens after elevated temperatures, high strength concrete grade among C60~C80 has little influence on the bond strength.
- (5) For specimen after elevated temperatures, bond damage occurs quite early and fast when in low temperature. The energy dissipation capacity of interface generally strengthens with the improvement of concrete strength, but declines with the increase of elevated temperature.
- (6) Both strain and stress of square steel tube present exponential distribution along tube length and reduce from the free end to the loading end. The more the load is, the more the corresponding bond stress is.
- (7) The constitutive model expression of bond slip by three-stage model fitting is able to response the tendency of *P-S* curve well. In addition, the constitutive model is just applied to square cross-section specimens with concrete strength between 60 and 80 MPa.

Acknowledgments

The authors gratefully acknowledge the financial support of this research provided by National Natural Science Foundation of China (No. 51578163 and 51268004), and the key project of Natural Science Foundation of Guangxi Province (Project No. 2016GXNSFDA380032), High Level Innovation Group and Outstanding Scholar Program Project of Guangxi High Education (No: [2017]38). The writers also appreciate the

assistance that was provided by Jianjia Chen and Jinjun Xu during the experimental process.

References

- AII (1997), Recommendations for design and construction of concrete filled steel tubular structure; Architectural Institute of Japan, Tokyo, Japan.
- Aslani, F., Uy, B. and Tao, Z. (2015), "Predicting the axial load capacity of high-strength concrete filled steel tubular columns", *Steel Compos. Struct., Int. J.*, **19**(4), 967-993.
- BS 540025 (2005), Steel concrete and composite bridges: Part 5: Code of Practice for the Design of Composite Bridges; British Standard Institute, London, Britain.
- BS EN 1994-1-1 (2004), Eurocode 4: Design of composite steel and concrete structures: Part 1.1, General rules and rules for buildings; British Standards Institution, London, Britain.
- Chiang, C.H. and Tsai, C.L. (2003), "Time-temperature analysis of bond strength of a rebar after fire exposure", *J. Cement Concrete Res.*, **33**(10), 1651-1654.
- Dong, C.X., Kwan, A.K.H. and Ho, J.C.M. (2015), "A constitutive model for predicting the lateral strain of confined concrete", *Eng. Struct.*, **91**, 155-166.
- El-Hawary, M.M. and Hamoush, S.A. (1996), "Bond shear modulus of reinforced concrete at high temperatures", *Eng. Fract. Mech.*, **55**(6), 991-999.
- Guler, S., Çopur, A. and Aydogan, M. (2014), "A comparative study on square and circular high strength concrete-filled steel tube columns", *Adv. Steel Constr.*, **10**(2), 234-247.
- Haddad, R.H. and Shannis, L.G. (2004), "Post-fire behavior of bond between high strength pozzolanic concrete and reinforcing steel", *Constr. Build. Mater.*, **18**(6), 425-435.
- Kwan, A.K.H., Dong, C.X. and Ho, J.C.M. (2015), "Axial and lateral stress-strain model for FRP confined concrete", *Eng. Struct.*, **99**, 285-295.
- Lai, M.H. and Ho, J.C.M. (2014), "Experimental and theoretical studies of confined HSCFST columns under uni-axial compression", *Earthq. Struct., Int. J.*, **7**(4), 527-552.
- Ma, Y.S. and Wang, Y.F. (2012), "Creep of high strength concrete filled steel tube columns", *Thin-Wall. Struct.*, **53**(2), 91-98.
- Moliner, V., Espinos, A. and Romero, M.L. (2013), "Fire behavior of eccentrically loaded slender high strength concrete-filled tubular columns", *J. Constr. Steel Res.*, **83**, 137-146.
- Patel, V.I., Liang, Q.Q. and Hadi, M.N.S. (2014), "Numerical analysis of high-strength concrete-filled steel tubular slender beam-columns under cyclic loading", *J. Constr. Steel Res.*, **92**(1), 183-194.
- Qu, X., Chen, Z. and Nethercot, D.A. (2014), "Push-out tests and bond strength of rectangular CFST columns", *Steel Compos. Struct., Int. J.*, **19**(1), 21-41.
- Romero, M.L., Espinos, A. and Portolés, J.M. (2015), "Slender double-tube ultra-high strength concrete-filled tubular columns under ambient temperature and fire", *Eng. Struct.*, **99**, 536-545.
- Schaumann, P., Kodur, V. and Bahr, O. (2009), "Fire behaviour of hollow structural section steel columns filled with high strength concrete", *J. Constr. Steel Constr.*, **65**(8-9), 1794-1802.
- Schaumann, P. and Kleibömer, I. (2017), "Experimental and numerical investigations of the composite behaviour in concrete-filled tubular columns with massive steel core at high temperatures", *J. Struct. Fire Eng.*, **9**(2), 147-160.
- Shakir-Khalil, H. (1993), "Push out strength of concrete-filled steel hollow sections", *Struct. Engr.*, **71**, 230-233.
- Song, T.Y., Tao, Z. and Han, L.H. (2017), "Bond behavior of concrete-filled steel tubes at elevated temperatures", *J. Struct. Eng.*, **143**(11), 04017147
- Su, Q.T., Yang, G.T. and Bradford, M.A. (2014), "Static behaviour

- of multi-row stud shear connectors in high-strength concrete”, *Steel Compos. Struct., Int. J.*, **17**(6), 967-980.
- Tao, Z., Han, L.H. and Uy, B. (2011), “Post-fire bond between the steel tube and concrete in concrete-filled steel tubular columns”, *J. Constr. Steel Res.*, **67**(3), 484-496.
- Tao, Z., Song, T.Y. and Uy, B. (2016), “Bond behavior in concrete-filled steel tubes”, *J. Constr. Steel Res.*, **120**, 81-93.
- Wang, Y.B. and Liew, J.Y.R. (2016), “Constitutive model for confined ultra-high strength concrete in steel tube”, *Constr. Build. Mater.*, **126**, 812-822.
- Xiong, M.X. and Liew, J.Y.R. (2016), “Mechanical behavior of ultra-high strength concrete at elevated temperatures and fire resistance of ultra-high strength concrete filled steel tubes”, *Mater. Des.*, **104**, 414-427.
- Xu, C., Huang, C.K. and Jiang, D.C. (2009), “Push-out test of pre-stressing concrete filled circular steel tube columns by means of expansive cement”, *Constr. Build. Mater.*, **23**(1), 491-497.
- Xu, J.J., Chen, Z.P. and Xue, J.Y. (2013), “Failure mechanism of interface bond behavior between circular steel tube and recycled aggregate concrete by push-out test”, *J. Build. Struct.*, **34**(7), 148-156. [In Chinese]
- Yang, Z., Li, G. and Lang, Y. (2017), “Flexural behavior of high strength concrete filled square steel tube with inner CFRP circular tube”, *Ksce J. Civil Eng.*, **21**(7), 2728-2737.